Corrosion Science 83 (2014) 367–374

Contents lists available at ScienceDirect

Corrosion Science

journal homepage: www.elsevier.com/locate/corsci

The hot forging behaviour and its effects on the oxidation behaviour of W–Cr alloy

Yunping Li [a,*], Peng Li [b], Huakang Bian [b], Ning Tang [a], Yuichiro Koizumi [a], Akihiko Chiba [a]

[a] Institute for Materials Research, Tohoku University, Sendai 980-8577, Japan
[b] Materials System Engineering, School of Engineering, Tohoku University, Sendai 980-8577, Japan

ARTICLE INFO

Article history:
Received 19 September 2013
Accepted 3 March 2014
Available online 11 March 2014

Keywords:
C. Interfaces
A. Alloy
C. Oxidation

ABSTRACT

For the first time, hot compression of a sintered W–20Cr–20Mo–1.5Pd alloy was performed to improve oxidation resistance. Residual pores in as-sintered alloy were hypothesized to be eliminated through sliding of the viscous Pd–Cr-containing grain boundary during compression at $10^{-4}\,s^{-1}$ and 1350 °C, which increased the alloy's oxidation resistance. Because of sufficient Cr from the Pd–Cr phase near the grain boundary after hot compression, Cr could transfer more efficiently into the Cr-depleted zone, and therefore, the oxide film/matrix interface was much stronger and showed fewer interfacial cracks than the as-sintered alloy did.

1. Introduction

The high melting point (3420 °C) of tungsten and its alloys make them extremely suitable for high-temperature applications. However, the applications of W and its alloys are limited because of their low oxidation resistance at high temperatures [1]. Alloying of W with active elements such as Cr, Ti, and Si that are preferentially oxidized to form a compact and continuous film such as Cr_2O_3 [2–5], TiO_2 [6], and SiO_2 [7,8], respectively, prevents progression of inward oxidation since the oxide films act as a barrier. Among these alloys, W–Cr-based alloys have been preferred, owing to their outstanding mechanical properties and oxidation resistance at high temperatures. W–Cr alloys are generally produced by the powder metallurgy process, where densification of the alloy is realized via sintering the W–Cr powder at high temperatures in a reducing environment [2–5,9]. However, the sintering ability of W–Cr powder is extremely low due to the low inter-diffusion coefficient of W–Cr at high temperatures for diffusion of Cr in W and of W in Cr [10]. Insufficient sintering inevitably leads to the formation of a large number of residual pores along the triple junction of grain boundaries in the alloy matrix. As a result, not only the mechanical properties but also the oxidation resistance of the alloy deteriorates, since at high temperatures, the infiltration of O through the residual pores into the matrix easily leads to a catastrophic failure in the alloy matrix because of oxidation [11,12].

Preparing W–Cr powder composed of nanoparticles via high-energy ball milling has been proven to be effective in improving the sintering ability and in subsequently eliminating the residual pores by increasing the specific surface area of particles [9]. However, contamination by external elements incorporated during the long milling process has been a major concern for researchers [13,14]. Increasing sintering temperature and/or prolonging the duration of sintering on a large scale resulted in only limited improvement in the sintering ability of the powder, because a drastic loss of Cr content occurred owing to its evaporation above 1400 °C. A Cr–Pd (Cr_2Pd_3) phase with a melting point much lower than that of the W matrix is formed, and it provides an effective diffusion medium for both Cr and W. This proves that Pd is an efficient sintering activator for W–Cr alloys [15,16]. Pd also enhances the oxidation resistance of W–Cr alloy, since Pd along the grain boundaries can act as Cr reservoirs [17], as channels for outward diffusion of Cr to the sample surface, and as a barrier against the inward diffusion of O [15]. Nevertheless, the abovementioned sintering defects such as residual pores and non-homogeneous microstructure could not be completely eliminated owing to the extremely large difference in melting points of W and the other elements.

Hot forging is an effective technique to optimize the microstructure of metallic materials [18,19]. At suitable conditions, the residual pores generated during casting or heat treatment (e.g., hot forging) of alloys can be effectively eliminated, and a more uniform microstructure can be realized, because of the plastic flow of crystalline grains driven by external stress, dynamic recrystallization (DRX), and dynamic recovery (DRV). However, since a very

* Corresponding author.
E-mail address: lyping@imr.tohoku.ac.jp (Y. Li).

http://dx.doi.org/10.1016/j.corsci.2014.03.005
0010-938X/

high temperature is required for hot forging of W-based alloys because of the extremely high melting point of W [1], to the best of our knowledge, there has been no reported research on the effects of hot forging on the properties of W-based alloys.

In the present research, hot-forging tests on a conventionally sintered W–20Cr–20Mo–1.5Pd alloy workpiece were carried out using a computer-aided hot-forging simulator. Microstructure evolution and plastic-deformation mechanisms were evaluated in detail. In addition, the influence of hot forging on the oxidation resistance of this alloy was analyzed in detail for the first time. The results are expected to facilitate the development of W-based alloys with enhanced properties.

2. Experimental procedures

W–Cr–Mo–Pd alloys having a nominal composition of W–20Cr–20Mo–1.5Pd (wt%) were used in the present study. Alloys with a relative density of 93.2% were consolidated by conventional sintering methods in a reducing hydrogen (H_2) atmosphere. Using the following equation, the theoretical density of a fully densified W–20Cr–20Mo–1.5Pd alloy was calculated to be 12.73 g/cm^3, by assuming that no volumetric change due to the formation of a solid solution and precipitation of a second phase occurred:

$$\rho = \frac{m(W) + m(Cr) + m(Mo) + m(Pd)}{\frac{m(W)}{\rho(W)} + \frac{m(Cr)}{\rho(Cr)} + \frac{m(Mo)}{\rho(Mo)} + \frac{m(Pd)}{\rho(Pd)}} \quad (1)$$

where $m(W) = 60$ g, $m(Cr) = 20$ g, $m(Mo) = 20$ g, and $m(Pd) = 1.5$ g, which are the mass of each element when the overall mass of sample is 101.5 g. The densities of W, Cr, Mo, and Pd-ρ(W), ρ(Cr), ρ(Mo), and ρ(Pd)—are 19.27, 7.20, 10.22, and 12.00 g/cm^3, respectively.

Using a computer-aided ThermecMastor-Z hot-forging simulator, hot compression was carried out in vacuum at temperatures of 1250–1400 °C; the temperature was increased at steps of 50 °C. A cylindrical specimen 8 mm in diameter and 12 mm in height was used for the hot-compression test. The selected strain rates were 10^{-4}, 3×10^{-4}, 10^{-3}, 3×10^{-3}, and 10^{-2} s^{-1}. The final reduction ratio for the sample after hot compression was approximately 30%. Before hot compression, the specimens were heated to the target temperature at the rate of 5 °C s^{-1} by high-frequency induction, and their temperature was maintained constant for 300 s in order to ensure uniform temperature throughout the specimens. Immediately after hot compression to the final strain level, the specimens were quenched to room temperature with high-pressure He gas (approximately 0.5 MPa) at a cooling rate of 50 °C s^{-1}. A cylindrical die made of Si_3N_4, with a diameter of 20 mm and height of 40 mm was used during the hot compression.

Sheet specimens with a size of 6 mm × 10 mm × 1 mm cut from both the as-sintered and the hot-compressed samples were abraded to 1500 grit finish and ultrasonically cleaned in acetone and then in methanol. Cyclic oxidation tests were performed at 800 °C, 900 °C, and 1000 °C in air using a muffle furnace (Muffle Furnace FO200, Yamato & Co, Tokyo, Japan). The tests involved placing the specimens in alumina crucibles and exposing them to the test temperature for 1 h and then air-cooling them to room temperature. The changes in weight were measured using a semi-microbalance (AUW320, Shimadzu, Tokyo, Japan) with an accuracy of ±0.1 mg. The cumulative time of exposure at the chosen temperature was 25 h.

Oxidation resistance of both as-sintered and hot-forged samples were evaluated using the weight gain of the samples, according to the following equation:

$$\Delta m = \frac{m_0 - m_i}{A_0}, \quad (2)$$

where Δm is the weight gain of the sample; m_0 and m_i are the masses of the sample before and after the oxidation test, respectively, for a given duration; and A_0 is the surface area of sample before the oxidation test. Microstructural observation and compositional analysis were carried out using a field-emission scanning electron microscope (FE-SEM) and energy dispersive X-ray spectroscopy (EDX) integrated on the FE-SEM equipment (JEOL Ltd., Peabody, Massachusetts, USA). Observation of the microstructure at the centre of the compressed samples was also carried out using electron backscatter diffraction (EBSD) equipment equipped with data acquisition software (TSL-OIM 5.0). X-ray diffraction (XRD) measurements for the phase characterization of samples before and after oxidation were carried out using a Philips X'Pert MPD diffractometer with a Cu Kα radiation source having a wavelength of 0.1542 nm and operated at 45 kV and 40 mA.

3. Results

3.1. Initial microstructure

The SEI image of the as-sintered sample in Fig. 1(a) indicates that the alloy produced by powder metallurgy has equiaxed crystalline grains ranging from 3 to 5 μm. Following polishing and cleaning, the grain boundaries are clearly visible, and a number of black spots smaller than 1 μm in diameter around the triple junctions of the grain boundary are confirmed to be residual closed pores owing to insufficient sintering. Corresponding elemental distribution maps of Cr and Pd by EPMA measurements are shown in Fig. 1(b) and (c), respectively. It can be seen that Pd exists along the grain boundary together with Cr with an area fraction of approximately 3.5%, although the fraction for Cr is not significant. XRD measurement on the as-sintered sample revealed a bi-phased alloy with an alloying W matrix peak and Cr_2Pd_3 peak; this indicates that a part of the Pd and Cr contents formed the intermetallic compound Cr_2Pd_3 in the vicinity of the grain boundary (see Fig. 2)

3.2. Hot compression behaviour

Fig. 3 shows the true stress–true strain curves of the W–20Cr–20Mo–1.5Pd alloy after hot compression at various strain rates at 1350 °C (a) and at various temperatures with a strain rate of 10^{-4} s^{-1} (b). It can be seen that at a strain rate of 10^{-4} s^{-1}, the

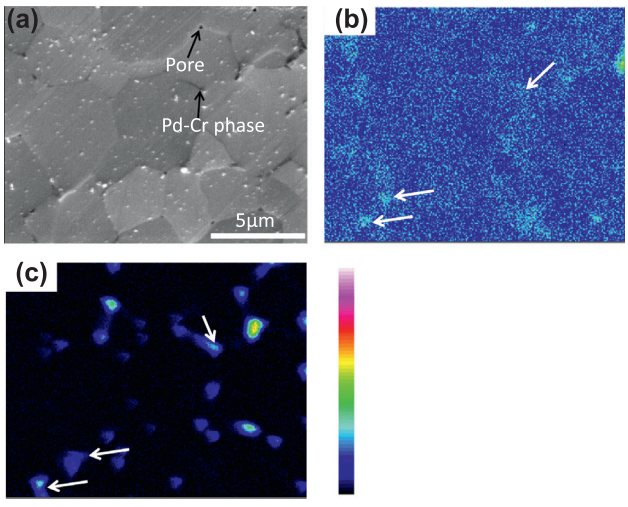

Fig. 1. Initial microstructure of the W–20Cr–20Mo–1.5Pd alloy produced by powder metallurgy: (a) SEI image; (b) elemental distributions of Cr and (c) Pd measured by EPMA.